

Doped HfO_x Nanoclusters: Polar and Resistive Switching in the Smallest Functional Units

Konstantin Z. Rushchanskii,* Marjana Ležaić, and Stefan Blügel

In the study presented in this article, the impact of proton doping on the structural and electronic properties of hafnium oxide nanoclusters is investigated, with a focus on their potential for use in resistive and polar switching devices. In the results, it is shown that the incorporation of protons can stabilize the cage-like crystalline structures of Hf_6O_x clusters, leading to reversible changes in electronic properties by varying oxygen stoichiometry. However, the full coverage of hafnia atoms by hydrogen removes in-gap states, highlighting the importance of controlled moisture content in redox-based memristive devices and neuromorphic units. In addition, in this study, the polar properties of these clusters are explored, illustrating possible polar switching in metastable pure Hf_6O_9 , low-barrier anti-ferroelectric-like switching in carbon-stabilized $\text{Hf}_6\text{O}_9:\text{C}$, and low-barrier polar switching in $\text{Hf}_{10}\text{O}_{15}:\text{C}$. In these findings, the potential of HfO_x clusters is revealed as active components for next-generation high-capacity nonvolatile electronic memory and beyond von Neumann computing in sub-nanometer scale.

1. Introduction

Redox-based memristive (ReRAM) devices have garnered significant attention in recent years for their potential as nonvolatile memories, selector devices, and building blocks for neuromorphic computing. Hafnium oxide (HfO_2)^[1] has emerged as a promising active material for future nanoelectronic devices due to its compatibility with state-of-the-art complementary metal-oxide semiconductor (CMOS) processes,^[2–4] as well as with resistive switching^[5,6] and ferroelectricity at the nanoscale.^[7–9] HfO_2 is already being used in a variety of nanoelectronic applications, including metal-oxide semiconductor field-effect transistors, ferroelectric field-effect transistors, highly scaled dynamic random-access memories, and ReRAM devices. To achieve next-generation


high-capacity nonvolatile electronic memory, it is essential to scale the functionality of active materials down to nanometer-sized thin films as well as up to individual nanocrystals between two nanosized electrodes.

Hafnia nanoparticles have already generated significant interest in the commercial and application domains due to their unique properties and potential for various technological applications. The small size and high surface area of these nanoparticles make them attractive for applications such as catalysis.^[10] Additionally, they exhibit a high transmittance over a wide wavelength range, hydrophobic nature, and hardness that represent an important combination required in optical coatings.^[11] Furthermore, hafnia nanoparticles have been proposed for use as radio enhancers to improve cancer cell eradication by augmenting the photoelectric

cross section of targeted cancer cells relative to the healthy surroundings.^[12] Their eco-friendly nature advances their use in wearable ink-jet-printed electronics^[13] and for energy storage.^[14] In addition, hafnia nanoparticles have shown promise as a coating material for enhancing the durability of biomedical implants, fuel cells, and solar cells. The HfO_2 -based nanostructures can be well manipulated by modulating the synthesis parameters resulting in assemblies of different types, such as hollow spheres, solid spheres, yolk-shells, aggregations, and defect-rich nanoparticles.^[15] Highly ordered HfO_2 nanoparticle nanoribbon assemblies with resistive switching properties tunable by varying organic ligand type were recently reported.^[16] With ongoing research and development, the potential applications of hafnia nanoparticles are expected to expand further, making them a promising material for future technological advancements.

Recent research^[17] has identified small HfO_x nanoislands grown by van der Waals epitaxy on graphite substrate. Experimental scanning tunneling microscopy (STM) images were compared with the theoretically predicted crystalline structures of the most stable nanoclusters. Under the applied growth conditions, the incorporation of C atoms during nanoclusters nucleation is energetically favorable over the formation of pure Hf_mO_n for selected cluster sizes with $m = 5$ and 6. Simulated STM images of these clusters allowed to identify $\text{Hf}_6\text{O}_{10}:\text{C}$ (as well as $\text{Hf}_{10}\text{O}_{16}:\text{2C}$ corresponding to two merged $\text{Hf}_6\text{O}_{10}:\text{C}$ clusters) and the Hf_4O_7 ones. Together with Hf_5O_8 and $\text{Hf}_5\text{O}_8:\text{C}$, these clusters build basic structural units that recur in larger clusters during the growth process. Moreover, carbon incorporation was found to be a source of an in-gap state observed for small Hf_mO_n clusters, in addition to the states related to

K. Z. Rushchanskii, M. Ležaić, S. Blügel
 Peter Grünberg Institut (PGI-1) and Institute for Advanced Simulation (IAS-1)
 Forschungszentrum Jülich and JARA-FIT
 52425 Jülich, Germany
 E-mail: k.rushchanskii@fz-juelich.de

 The ORCID identification number(s) for the author(s) of this article can be found under <https://doi.org/10.1002/pssa.202300404>.

© 2023 The Authors. physica status solidi (a) applications and materials science published by Wiley-VCH GmbH. This is an open access article under the terms of the Creative Commons Attribution-NonCommercial License, which permits use, distribution and reproduction in any medium, provided the original work is properly cited and is not used for commercial purposes.

DOI: 10.1002/pssa.202300404

clusters' oxygen stoichiometry, revealing acceptor- and donor-like in-gap states in addition to the bulk-like band gap.^[18]

Despite the significant variability in the crystalline structure of the clusters, a limited number of surface and defect-related in-gap states were revealed through differential conductance spectroscopy combined with ab initio hybrid-functional calculations of the clusters' electronic states.^[17] These states can be classified based on their origin, as follows: two surface states were attributed to i) a delocalized state over oxygen atoms bridging two hafnium atoms and ii) an apical oxygen atom singly bound to a hafnium atom. Additionally, two defect states related to the formation of oxygen vacancies in HfO_x nanoclusters were represented by i) a largely delocalized orbital with an energy below the Fermi level and ii) an unoccupied orbital delocalized over threefold coordinated hafnium atoms in sub-stoichiometric Hf_mO_n clusters. The latter defect states correspond well to defect bands referred to as deep and shallow defects in oxygen-deficient hafnia thin films typically used in ReRAM devices.^[18] These findings regarding defect states are not limited to the nanoclusters only, but might also be significant near the surfaces of grains or in the amorphous state of hafnia.

The resistive hysteresis in HfO_2 -based ReRAM devices is attributed to the migration of oxygen vacancies^[5,19] and redox reactions induced by an applied electric field, while the ferroelectricity is related to the metastable (MS) polar orthorhombic phase.^[2,20] Despite considerable progress in understanding the switching mechanism and enhancing the device performance, large variability in both properties remains a significant issue. In particular, limited retention and endurance^[21] are crucial for resistive switching devices, whereas wake-up and fatigue regimes^[22] are essential for the ones based on polar switching. Therefore, a microscopic model of the system, based on possible minimal structural units, can offer valuable insight into the impact of oxygen vacancies or dopants on the performance of the active oxide in the (poly)crystalline or amorphous state, especially in the vicinity of the ultimate scaling limit.

In this article, we investigate the stability of small clusters in the presence of hydrogen atoms. The choice of hydrogen atoms as dopants was made for several reasons. First, a proton is the smallest component that can be added to the cluster structure, and can therefore fit into the sites where other dopants cannot. Additionally, it carries an elementary charge, which allows external charge to be easily controlled by adjusting the amount of protons added. From an experimental standpoint, uncontrolled proton doping might be important when the organic molecules are used as precursors for hafnia synthesis,^[23] as well as in the presence of moisture.^[24] Hydrogen is commonly used in silicon technology as a reducing agent during epitaxial growth, etching, annealing, and passivation of the silicon surface. Therefore, understanding the role of hydrogen on the structural properties of small hafnia clusters may provide valuable information for integrating hafnia functional oxides with state-of-the-art CMOS processes. Regarding the resistive switching in hafnia-based devices, moisture has been identified as a source of variability of ReRAM devices,^[24] as it can be absorbed from the local environment or during device fabrication, providing additional charges in the oxide matrix and enhancing ion diffusion, while also acting as a corrosive agent. Therefore, understanding the interaction of protons with the HfO_x clusters may provide

significant insight into the structural preferences during the nucleation processes, as well as the mediation of electronic properties. We will show that despite being the source of variability in functional ReRAM devices, protons stabilize the atomic structure of small nanoclusters over a wide range of H and O concentrations, whereas variability in electronic properties is strongly affected by changes in H and O concentrations, as well as by their ratio.

We also show how the presence of H affects the polar distortion in small clusters and investigate polar switching properties in the smallest possible functional unit of hafnia.

2. The Role of Hydrogen in the Stability of Small HfO_x Clusters

To gain a detailed understanding of how hydrogen is incorporated into small hafnia clusters, we utilized an evolutionary algorithm^[25–27] combined with ab initio calculations, to predict the crystalline structures of Hf_4O_x , Hf_5O_x , and Hf_6O_x clusters with varying numbers of hydrogen atoms in the vicinity of the lowest energy stable structures. The energy of formation, scaled per atom, is presented in **Figure 1** as a function of oxygen content. In this diagram, we used athermal conditions, where the chemical potential of oxygen is taken with respect to a spin-polarized single oxygen molecule in an empty box, and the chemical potential of hydrogen is taken with respect to a spin-polarized free-standing atom. These conditions differ from those used in ref. [17] to mimic experimental conditions, but the differences for the undoped clusters are seen only for Hf_4O_x structures, where the stoichiometric Hf_4O_8 is the most stable atomic configuration. The most stable larger clusters, Hf_5O_9 and Hf_6O_{12} , are the same as those in ref. [17].

The local structure of small Hf_4O_x clusters changes significantly with the oxygen content. We found that substoichiometric compositions tend to form compact, symmetric packing, which is observed in the high-temperature phases of bulk hafnia.^[7,20,22,28] In contrast, the stoichiometric Hf_4O_8 cluster exhibits anisotropic atomic arrangements that reflect the local structure of the Baddeleyite monoclinic phase^[29] (see **Figure 2**). These results are consistent with our recent investigation of substoichiometric hafnia, where we predicted the stabilization of a fluorite-like crystalline structure via ordered oxygen vacancies.^[30,31] In the following, we refer to the atomic arrangements in Hf_4O_7 as fluorite-like structural unit (FSU) and the arrangement in Hf_4O_8 as Baddeleyite structural unit (BSU). As shown in **Figure 2**, these two arrangements are common building blocks for larger clusters. The structure of Hf_5O_9 , which is the most stable among Hf_5O_x clusters, is based on the FSU, while the stoichiometric Hf_5O_{10} has the BSU at its origin. Here, the reduced Hf_5O_8 cluster begins to deviate from bulk-like arrangements, revealing a cage-like structure (see **Figure 2b**). For even larger Hf_6O_x clusters (see **Figure 2c**), the trend is similar, with substoichiometric Hf_6O_{10} exhibiting FSU units, and MS stoichiometric Hf_6O_{12} exhibiting BSU units. The energy difference of MS configuration to the ground-state atomic arrangements is only 12.8 meV per atoms. However, the structures of the Hf_6O_{11} and the ground-state Hf_6O_{12} clusters clearly indicate their origin to be based on the cage-like Hf_5O_8 one with extra oxygen in the

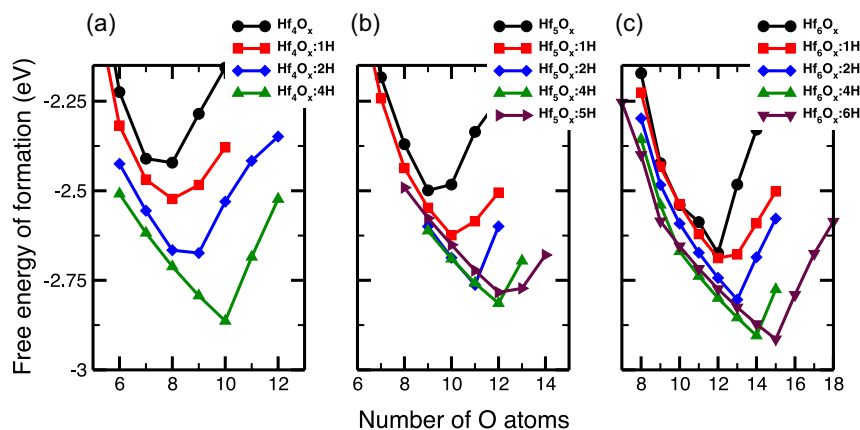


Figure 1. Free energy of formation diagram (per atom) of small a) Hf_4O_x , b) Hf_5O_x , c) Hf_6O_x clusters as a function of the amount of oxygen and in the presence of H dopants.

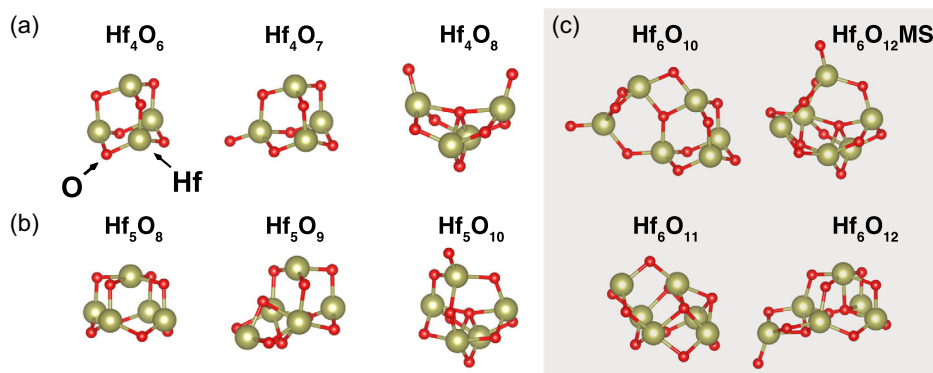


Figure 2. Structures of small a) Hf_4O_x , b) Hf_5O_x , and c) Hf_6O_x -undoped clusters around their free energy of formation minima. The structures of Hf_6O_x clusters are given in shaded area in the corresponding row of smaller cluster to compare common structural units. Hf_6O_{12} stands for the calculated ground-state structure, whereas the Hf_6O_{12} MS shows the first MS nanoparticle configuration. The ground-state structures of Hf_6O_{12} as well as Hf_5O_{10} originate from the structure of Hf_4O_8 nanocluster, whereas the Hf_6O_{11} and the Hf_6O_{12} clusters have building blocks of the Hf_5O_8 nanoparticle. The Hf_5O_9 and Hf_6O_{10} clusters have common blocks with Hf_4O_7 . The structure of Hf_6O_9 nanoparticle is presented in Figure 6a, together with the polar switching path.

cage center. The variability of atomic arrangements in Hf_6O_x cluster is irregular with respect to the oxidation level, as the general trend of monoclinic-like BSU changing to fluorite-like FSU and then to amorphous-like cage structure is lost: the stoichiometric Hf_6O_{12} and slightly reduced Hf_6O_{11} have a rather cage-like structure, which might indicate the first nucleation of the amorphous state. The strongly reduced Hf_6O_9 again reveals the cage-like structure, which originates from the structure of Hf_6O_{11} (compare the structure with the one in Figure 6a).

The cage-like structural units (CSUs) are more suited for doping with foreign atoms than the compact BSU and FSU. In fact, as mentioned in Introduction, when doped with C atoms, the $\text{Hf}_5\text{O}_8:\text{C}$ and $\text{Hf}_6\text{O}_{10}:\text{C}$ CSU structures were found to be the most stable atomic arrangements, from which the $\text{Hf}_6\text{O}_{10}:\text{C}$ -based clusters were experimentally revealed in ref. [17].

In the following, we will focus on the stability of HfO_x clusters in the presence of H atoms, and their electronic properties, which we will present in terms of highest-occupied molecular orbital and lowest unoccupied molecular orbital (HOMO–LUMO gap). Although the exact information about the electronic conductivity, which is mediated by tunneling current from or

to the in-gap states of the clusters, significantly depends on the position of these states relative to the Fermi level, which, in turn, is defined by electrodes material and depends on the interaction of nanoparticle with electrode/substrate, the aim of this article is to illustrate the general trends in electronic properties of clusters as a function of oxygen content. For resistive switching, these trends are sufficiently captured by comparing the HOMO–LUMO gap values of nanoclusters at different oxidation states.

In contrast to C atoms, which are incorporated to the center of the CSU, hydrogen atoms tend to decorate the outer shell of clusters by making single bonds with Hf atoms. This observation holds for all considered clusters, as shown in Figure 3 and 4. Hence, we did not consider cases with an excess of H over the number of Hf atoms in the clusters. In extremely reduced regimes, H atom can replace missing oxygen atoms to form a bridge connecting two Hf atoms, for instance, in $\text{Hf}_4\text{O}_4:\text{H}$ (not shown) or in $\text{Hf}_6\text{O}_8:6\text{H}$ (shown in Figure 4d). Although this substitution significantly narrows the HOMO–LUMO gap (see Figure 5 for $\text{Hf}_6\text{O}_x:6\text{H}$ clusters) and might be desirable for resistive switching, the formation energy for such a configuration is significantly higher than the stable configuration

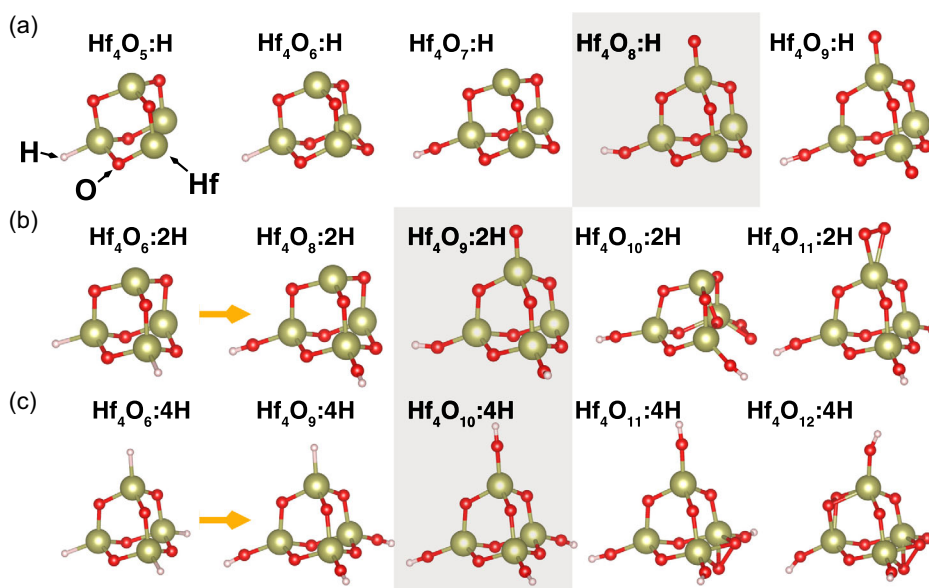


Figure 3. The structure of minimal Hf_4O_x clusters, stabilized by a) one, b) two, and c) four H atoms. Orange arrows indicate continuous increase of oxygen content, which results in formation of Hf–OH bonds. Shaded area indicates the most stable structures.

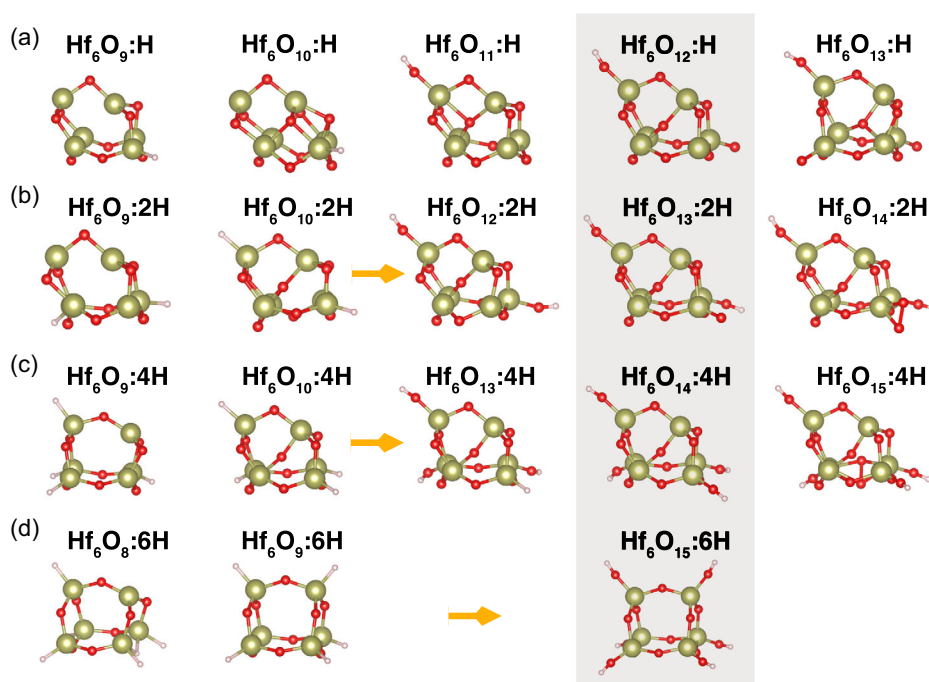


Figure 4. The cage structure of Hf_6O_x clusters, stabilized by a) one, b) two, c) four, and d) six H atoms. The meaning of symbols is the same as in Figure 3.

(see Figure 1). Moreover, kinetically, substitution of atoms in the stable frame appears to be more complex than passivation reaction on the Hf atoms.

For all H concentrations, the presence of protons eliminates the formation of BSU structures in small Hf_4O_x clusters, favoring the FSU one, which is the building block for tetragonal and

cubic phases of bulk hafnia. The stoichiometric configuration $\text{Hf}_4\text{O}_8:\text{H}$ can be considered as a substoichiometric BSU of Hf_4O_7 with hydroxyl group attached to one Hf atom. The oxidation of the $\text{Hf}_4\text{O}_6:\text{H}$ cluster to the $\text{Hf}_4\text{O}_7:\text{H}$ structure also occurs as the formation of a hydroxyl group in place of the Hf–H bond. This trend is general: the presence of protons helps

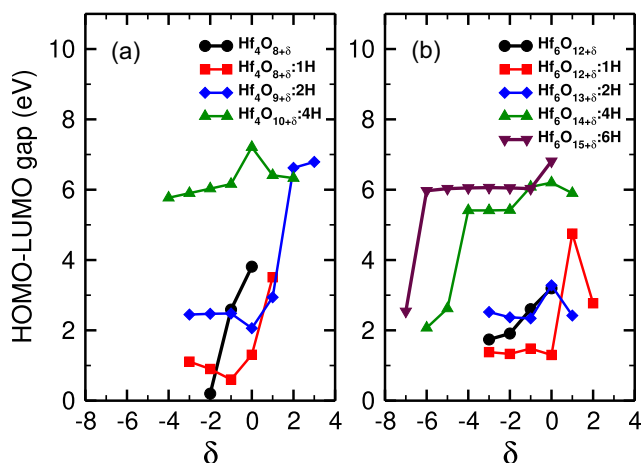


Figure 5. Calculated highest-occupied molecular orbital and lowest unoccupied molecular orbital gap for a) Hf_4O_x and b) Hf_6O_x clusters doped with various H atoms. Diagrams are given in coordinates, where δ describes oxygen off-stoichiometry relative to the most stable clusters with different hydrogen content.

to adsorb excess oxygen atoms by forming hydroxyl groups, while the basic structural frame remains unaffected. After saturation of all Hf–H bonds, further excess of oxygen atoms result in the formation of O_2 molecules adsorbed onto single Hf atoms (see $\text{Hf}_4\text{O}_{11}:2\text{H}$, $\text{Hf}_4\text{O}_{11}:4\text{H}$, and $\text{Hf}_4\text{O}_{12}:4\text{H}$).

For Hf_6O_x clusters (see Figure 4), the influence of H is more complicated. Generally, the frame resembles the same shape, seen in ref. [17] by doping with C (also, compare with Figure 6b). This shape is most obviously seen in the case of reduced $\text{Hf}_6\text{O}_9:\text{H}$, $\text{Hf}_6\text{O}_9:2\text{H}$, and $\text{Hf}_6\text{O}_9:4\text{H}$. The inner part of the CSU remains empty. It also remains empty in the case of full coverage of Hf_6O_x clusters with six H atoms, in all considered ranges of oxidation (see Figure 4d). When the oxygen content increases, one oxygen atom occupies the inner part of CSU, with only one exception, $\text{Hf}_6\text{O}_{10}:\text{H}$, which resembles the frame of undoped Hf_6O_{11} , described earlier. The variation in oxidation state is coherent with formation of hydroxyl groups in place of Hf–H bonds. After saturation of Hf–H bonds, further oxidation is still possible by the formation of adsorbed O_2 molecules to Hf (see $\text{Hf}_6\text{O}_{14}:2\text{H}$ and $\text{Hf}_6\text{O}_{15}:4\text{H}$ in Figure 4), similar to Hf_4O_x clusters. In the range of oxidation of the Hf–H bonds, the free energy of formation changes linearly with the content of oxygen (see Figure 1). The formation of adsorbed O_2 molecules leads to an increase in the formation energy and defines the position of energetically most stable configurations, which are the ones with fully saturated Hf–OH groups (see shaded areas in Figure 3 and 4). Note that the relative stability of the clusters depends on the chemical potential of oxygen and hydrogen, with a tendency to stabilize reduced clusters in an oxygen-poor environment.

The structure of doped Hf_6O_x clusters reveals deformed frames, unless they are fully covered with six hydrogen atoms (compare Figure 4a–c with 4d). This deformation is static in nature and may favor the nucleation of the polar phase during

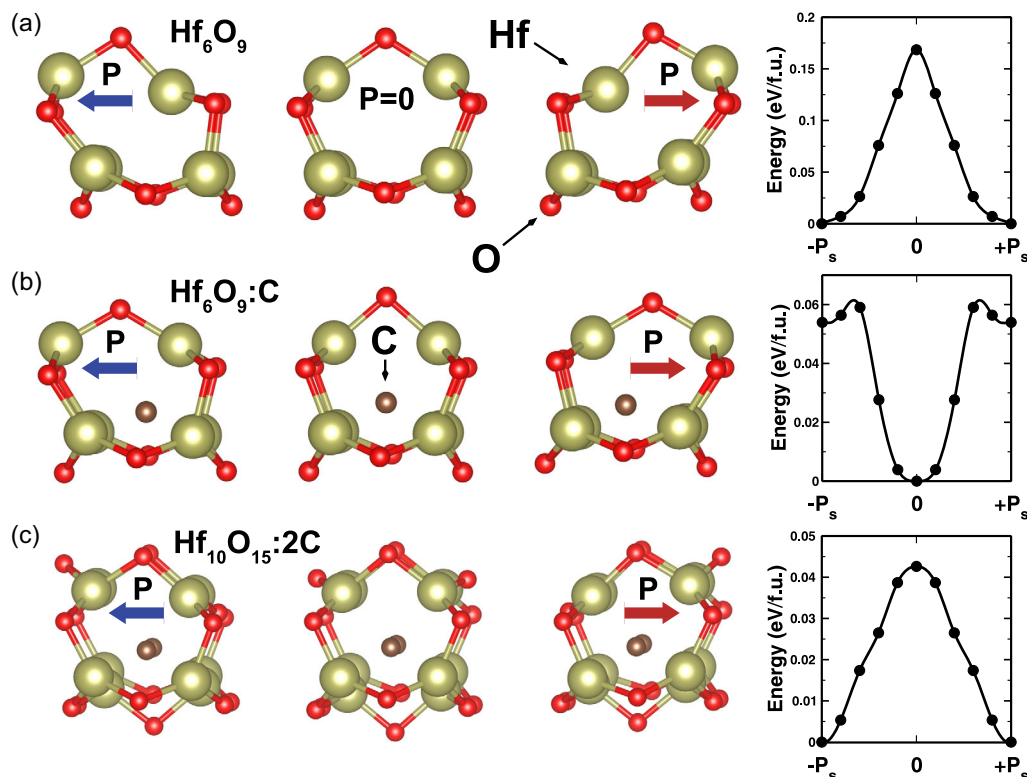


Figure 6. Schematic diagrams and corresponding energy barriers for polar switching in a) undoped cluster, b) cluster doped with C atom, and c) two adjacent clusters doped with C. Energy is given in eV per Hf atom. Switching in C-doped single-cluster $\text{Hf}_6\text{O}_9:\text{C}$ reveals antiferroelectric-like behavior, with minimum in undistorted configuration and local metastable minima in deformed polar cases.

crystal growth. The possible switching of polarity in these clusters is discussed in the next section. However, fully covered $\text{Hf}_6\text{O}_x\cdot 6\text{H}$ clusters are symmetric, losing the polar distortion of the frame.

For doped Hf_5O_x clusters, the energy minimum is higher than for the doped Hf_4O_x and Hf_6O_x clusters, indicating their thermodynamic instability. Indeed, the crystalline structures of Hf_5O_x clusters show strong inhomogeneities, including the presence of H. Therefore, considering their instability, they are not discussed in this article.

Next, we will discuss the correlation between the aforementioned structural changes and the size of the HOMO–LUMO gap (referred to simply as “gap” in the following), to address the changes in electronic properties of clusters with their oxidation state. In Figure 5, we clearly see that the $\text{Hf}_4\text{O}_x\cdot 4\text{H}$ and $\text{Hf}_6\text{O}_x\cdot 6\text{H}$ clusters, fully covered by H, reveal only subtle changes in the gap, as is expected for passivated cluster surface, because the $-\text{OH}$ states fall far below the HOMO level. Although this is not desirable for resistive switching, passivation assures a bulk-like value of the gap (≈ 6 eV) for even extremely small clusters, which have smaller gap in the undoped configuration. A remarkable functionality of these fully passivated clusters is their ability to adsorb excess oxygen, which significantly exceeds the stoichiometric composition, for example, from $\text{Hf}_4\text{O}_6\cdot 4\text{H}$ to $\text{Hf}_4\text{O}_{10}\cdot 4\text{H}$ and from $\text{Hf}_6\text{O}_9\cdot 6\text{H}$ to $\text{Hf}_6\text{O}_{15}\cdot 6\text{H}$. From this point of view, fully hydrogen-covered clusters might function as a sink or source for oxygen without changing their electronic properties.

Contrary to fully passivated cluster, adding only a single hydrogen atom represents another extreme case where the gap becomes significantly smaller comparing to undoped clusters (Figure 5). While the gap changes in reduced clusters are small compared to equilibrium conditions, this regime could be important for a forming step in thin-film devices, decreasing the voltage needed for filament formation, and making the gap almost independent on the cluster's oxidation state in its reduced state. Moreover, the slight increase in the gap observed in $\text{Hf}_4\text{O}_6\cdot \text{H}$ cluster when compared to the $\text{Hf}_4\text{O}_7\cdot \text{H}$ one might autocorrect the current in redox process preventing its heating and stopping possible avalanche instabilities. A significant decrease in the gap is observed when only one apical oxygen is removed from equilibrium configuration, while the hydroxyl group remains unaffected, as seen in the Figure 3a for $\text{Hf}_4\text{O}_7\cdot \text{H}$ comparing to $\text{Hf}_4\text{O}_8\cdot \text{H}$. Similar observations are valid for $\text{Hf}_6\text{O}_{11}\cdot \text{H}$ compared to $\text{Hf}_6\text{O}_{12}\cdot \text{H}$ (see Figure 4a), as well as for $\text{Hf}_4\text{O}_8\cdot 2\text{H}$ versus $\text{Hf}_4\text{O}_9\cdot 2\text{H}$ (Figure 3b), and for $\text{Hf}_6\text{O}_{12}\cdot 2\text{H}$ versus $\text{Hf}_6\text{O}_{13}\cdot \text{H}$ (Figure 4b).

For $\text{Hf}_6\text{O}_x\cdot 4\text{H}$, a significant decrease in the gap occurs when an oxygen atom is removed from the center of the CSU (compare $\text{Hf}_6\text{O}_9\cdot 4\text{H}$ with $\text{Hf}_6\text{O}_{10}\cdot 4\text{H}$ in Figure 4c). As in the case discussed earlier for $\text{Hf}_6\text{O}_8\cdot 6\text{H}$ versus $\text{Hf}_6\text{O}_9\cdot 6\text{H}$, this may be both kinetically and energetically challenging (see Figure 1).

As a brief summary of this section, we can conclude that adding a small amount of hydrogen decreases the gap compared to the undoped state, and increasing the hydrogen content systematically increases the gap while decreasing the gap variability.

It is worth noting that the diagrams in Figure 5 also demonstrate the gap dependence with respect to the variation of $-\text{OH}$ groups in the clusters.

3. Polar Switching in Hf_6O_x Cage-like Clusters

The asymmetric nature of the Hf_6O_x CSU results in an uncompensated electric dipole on the nanoparticle, which might mediate the spatial anisotropy of its chemical reactivity and aid in nucleating the polar phase. In this section, we will discuss the conditions under which the asymmetry of the clusters can be reversed, adding polar switching functionality to them, in addition to the discussed changes in electronic properties. The most stable structures, as discussed in the previous section (see shaded areas in Figure 4), contain one oxygen atom in the center of the cage, which forms bonds with three planar Hf atoms. To reverse the polarity of the clusters, the local arrangements of the central oxygen must be altered in such a way that the oxygen is reconnected to other three planar Hf atoms. However, these bonds are difficult to break, which results in a high transition barrier for switching the polarity. Moreover, the presence of apical H, O, and $-\text{OH}$ groups cause static distortions that require ionic movements to a new site on the cluster to switch the direction of the electric dipole.

The fully covered $\text{Hf}_6\text{O}_{15}\cdot 6\text{H}$ cluster is an exception in this sense, as it has an empty cage interior but a strong electrostatic interaction of external $-\text{OH}$ groups leads to a symmetric structure of the cluster, causing it to lose its polarity. The framework of this cluster can be seen as Hf_6O_9 core decorated by six $-\text{OH}$ groups. This is important because the Hf_6O_9 structure is strongly reduced form of pure hafnia with a polar distorted CSU, as shown in Figure 6a. This structure is realized in all considered concentrations of H atoms, as shown in Figure 4, for $\text{Hf}_6\text{O}_9\cdot \text{H}$, $\text{Hf}_6\text{O}_9\cdot 2\text{H}$, $\text{Hf}_6\text{O}_9\cdot 4\text{H}$, and $\text{Hf}_6\text{O}_9\cdot 6\text{H}$. Therefore, it is possible to grow the stable frame of the $\text{Hf}_6\text{O}_{15}\cdot 6\text{H}$ in an H- and O-rich atmosphere, followed by consequent annealing in a vacuum to remove the $-\text{OH}$ groups, leaving a pure Hf_6O_9 cluster. The cluster is predicted to exhibit ferroelectric-like switching with two states of electric dipole directions. The calculated transition barrier is relatively small, approximately 0.17 eV per Hf atom, which is similar to the one obtained by us for the vacancy-ordered polar orthorhombic phase in $\text{HfO}_{1.75}$.^[32]

Although the structure of the Hf_6O_9 cluster is predicted to have reasonable polar switching capability, its MS character plays against its crystalline stability, especially when exposed to an external oxygen-rich environment. From this perspective, the carbon-doped $\text{Hf}_6\text{O}_{10}\cdot \text{C}$ -based clusters with CSU, predicted and experimentally observed in ref. [17], look more promising. The $\text{Hf}_6\text{O}_{10}\cdot \text{C}$ itself possesses only static polarity due to the presence of apical oxygen. Calculated migration barrier for ionic movement of this oxygen to the site, compatible with opposite polarization, is ≈ 0.51 eV per Hf atom, which is high compared to the previous case. Reduction of the $\text{Hf}_6\text{O}_{10}\cdot \text{C}$ cluster to the $\text{Hf}_6\text{O}_9\cdot \text{C}$ one by removing the apical oxygen results in an undistorted frame (see Figure 6b). We found that elastic deformation of the shape of this frame results in two local minima with opposite direction of polarization, which might be switched solely by a displacement manner. The energy profile for this transition is antiferroelectric like, revealing ability of the cluster to store energy in its polarized state. Moreover, the energy barrier for this type of transition is only 0.06 eV per Hf atom, which is three times smaller than that for polar transition in Hf_6O_9 clusters. The formation energy for this reduced cluster is very close to

the most stable $\text{Hf}_6\text{O}_{10}:\text{C}$ one,^[17] which improves the stability of these clusters compared to undoped ones.

Finally, $\text{Hf}_6\text{O}_{10}:\text{C}$ clusters grown side by side, as experimentally revealed in ref. [17], can be reduced to the $\text{Hf}_{10}\text{O}_{15}:\text{2C}$ form, which exhibits ferroelectric-like behavior with a transition energy between two opposite state of polarization of only ≈ 0.042 eV per Hf atom.

4. Conclusion

In this study, we investigated the effect of incorporating protons into hafnium oxide nanoclusters on their structural and electronic properties. We also examined the functionality of small HfO_x clusters for resistive and polar switching devices. Our results demonstrate that the presence of H stabilizes cage-like crystalline structures of Hf_6O_x clusters, enabling reversal changes in electronic properties by varying oxygen stoichiometry. By introduction a small number of protons, the oxygen content can be varied in a wide range even beyond the normal stoichiometry of the clusters, allowing for stable resistive switching. However, we found that full coverage of hafnia atoms with hydrogen results in passivation of in-gap states, highlighting the importance of controlled moisture content in the ReRAM devices and neuromorphic units. In addition, we explored the polar properties of these clusters and demonstrated possible polar switching in MS pure Hf_6O_9 , low-barrier antiferroelectric-like switching in carbon-stabilized $\text{Hf}_6\text{O}_9:\text{C}$, and low-barrier polar switching in $\text{Hf}_{10}\text{O}_{15}:\text{C}$. Our findings reveal the smallest functional unit for resistive and ferroelectric switching in hafnia.

5. Experimental Section

Computational Details: For prediction of the ground-state structure of small clusters, we employed a global optimization method implemented as evolutionary algorithm in Universal Structure Predictor: Evolutionary Xtallography (USPEX) code.^[25–27,33] For structural relaxation and calculation of electronic properties, we used the all-electron projector-augmented-wave (PAW) method as implemented in Vienna abinitio simulation package.^[34–36] In our calculations, clusters were separated by a 7 Å thick vacuum space. To account for electron exchange and correlation, we utilized optimized for the molecules Perdew–Burke–Ernzerhof (PBE) functional.^[37] We used PAW_PBE pseudopotentials.^[38] The kinetic energy cutoff for the plane-wave basis set was limited to 600 eV. Structural optimization was performed until the Hellmann–Feynman force on each atom became less than $0.01 \text{ eV}\text{\AA}^{-1}$. We noted that PBE underestimated the HOMO–LUMO gap, and therefore, for comparison with experimental data, the electronic structures for selected clusters were calculated using the corrected Heyd–Scuseria–Ernzerhof (HSE06) hybrid functional.^[39]

Structure prediction of nanoparticles started from the randomly generated structures with various symmetries. After structural relaxation of randomly produced candidates, subsequent generations of structures was obtained using various mutation operators (heredity, permutation, soft mutation), applied to the 60% of the lowest-energy structures from the previous step. The ground-state structure was determined when it remained unchanged for a sufficient number of generations, typically 10–20, depending on the cluster size.

In calculations, we considered a vicinity of stoichiometric $\text{Hf}_m\text{O}_{2m(\pm\delta)}$ small clusters with $m = 4\text{--}6$ doped with k atoms of hydrogen with $k \leq m$. Free energy of formation was evaluated as

$$\Delta G_f = E(\text{Hf}_m\text{O}_n:k\text{H}) - mE(\text{Hf}_{\text{metal}}) - \frac{1}{2}nE(\text{O}_2) - kE(\text{H}) \quad (1)$$

where n is the number of oxygen atoms in the cluster; $E(\text{Hf}_m\text{O}_n:k\text{H})$ is the ground-state total energy of the Hf_mO_n cluster doped with k atoms of H; $E(\text{Hf}_{\text{metal}})$ is the chemical potential of Hf atom in its metallic form; $E(\text{O}_2)$ is the chemical potential of oxygen atom in O_2 molecule; and $E(\text{H})$ is the chemical potential of free-standing H atom.

Visualization was made with the help of Visualization for Electronic and Structural Analysis (VESTA) code.^[40] Computations were performed on JURECA supercomputer.^[41]

Acknowledgements

The authors gratefully acknowledge the financial support by Deutsche Forschungsgemeinschaft (DFG) through SFB 917 “Nanoswitches”, as well as the computing time granted through JARA on the supercomputer JURECA at Forschungszentrum Jülich and JARA-HPC Partition (project jara0126). The authors thank Dr. Ivetta Slipukhina for the critical reading of the manuscript and valuable suggestions. Open access funding enabled and organized by Projekt DEAL.

Open Access funding enabled and organized by Projekt DEAL.

Conflict of Interest

The authors declare no conflict of interest.

Data Availability Statement

The data that support the findings of this study are available from the corresponding author upon reasonable request.

Keywords

hafnia, nanoparticles, polar switching, resistive switching

Received: May 31, 2023

Revised: October 17, 2023

Published online: November 27, 2023

- [1] W. Banerjee, A. Kashir, S. Kamba, *Small* **2022**, *18*, 2107575.
- [2] N. Setter, D. Damjanovic, L. Eng, G. Fox, S. Gevorgian, S. Hong, A. Kingon, H. Kohlstedt, N. Y. Park, G. B. Stephenson, I. Stolitchnov, A. K. Tagansteve, D. V. Taylor, T. Yamada, S. Streiffer, *J. Appl. Phys.* **2006**, *100*, 051606.
- [3] F. Ali, X. Liu, D. Zhou, X. Yang, J. Xu, T. Schenk, J. Müller, U. Schroeder, F. Cao, X. Dong, *J. Appl. Phys.* **2017**, *122*, 144105.
- [4] S. Eaton, D. Butler, M. Parris, D. Wilson, H. McNeillie, *Dig. Tech. Pap.-IEEE Int. Solid-State Circuits Conf.* **1988**, *130*, 329.
- [5] M. Lanza, H.-S. P. Wong, E. Pop, D. Ielmini, D. Strukov, B. C. Regan, L. Larcher, M. A. Villena, J. J. Yang, L. Goux, A. Belmonte, Y. Yang, F. M. Puglisi, J. Kang, B. Magyari-Köpe, E. Yalon, A. Kenyon, M. Buckwell, A. Mehonic, A. Shluger, H. Li, T.-H. Hou, B. Hudec, D. Akinwande, R. Ge, S. Ambrogio, J. B. Roldan, E. Miranda, J. Suñe, K. L. Pey, et al., *Adv. Electron. Mater.* **2019**, *5*, 1800143.
- [6] L. Goux, P. Czarnecki, Y. Y. Chen, L. Pantisano, X. P. Wang, R. Degraeve, B. Govoreanu, M. Jurczak, D. J. Wouters, L. Altimime, *Appl. Phys. Lett.* **2010**, *97*, 243509.
- [7] T. S. Böschke, J. Müller, D. Bräuhäus, U. Schröder, U. Böttger, *Appl. Phys. Lett.* **2011**, *99*, 102903.
- [8] B. Noheda, P. Nukala, M. Acuautila, *Nat. Mater.* **2023**, *22*, 562.
- [9] X. Tian, S. Shibayama, T. Nishimura, T. Yajima, S. Migita, A. Toriumi, *Appl. Phys. Lett.* **2018**, *112*, 102902.

- [10] D. Laishram, K. P. Shejale, R. Gupta, R. K. Sharma, *ACS Sustainable Chem. Eng.* **2018**, 6, 11286.
- [11] A. Wiatrowski, A. Obstarczyk, M. Mazur, D. Kaczmarek, D. Wojcieszak, *Coatings* **2019**, 9, 2.
- [12] L. R. H. Gerken, A. L. Neuer, P. M. Gschwend, K. Keevend, A. Gogos, A. H. C. Anthis, L. Aengenheister, S. E. Pratsinis, L. Plasswilm, I. K. Herrmann, *Chem. Mater.* **2021**, 33, 3098.
- [13] G. Vescio, J. Lopez-Vidrier, R. Leghrib, A. Cornet, A. Cirera, *J. Mater. Chem. C* **2016**, 4, 1804.
- [14] J. Murugasamy, N. Ramalakshmi, R. Pandiyan, S. Ayyaru, V. Jayaraman, Y.-H. Ahn, *Inorg. Chem. Commun.* **2022**, 141, 109615.
- [15] H. Wang, D. Sun, Q. Lu, F. Wang, L. Zhao, Z. Zhang, X. Wang, H. Liu, *Nanoscale* **2019**, 11, 5240.
- [16] J. Wang, S. Choudhary, J. De Roo, K. De Keukeleere, I. Van Driessche, A. J. Crosby, S. S. Nonnenmann, *ACS Appl. Mater. Interfaces* **2018**, 10, 4824.
- [17] N. Schmidt, K. Z. Rushchanskii, U. Trstenjak, R. Dittmann, S. Karthäuser, *ACS Appl. Nano Mater.* **2023**, 6, 148.
- [18] Y. Y. Illarionov, T. Knobloch, M. Jech, M. Lanza, D. Akinwande, M. I. Vexler, T. Mueller, M. C. Lemme, G. Fiori, F. Schwierz, T. Grasser, *Nat. Commun.* **2020**, 11, 3385.
- [19] R. Waser, M. Aono, *Nat. Mater.* **2007**, 6, 833.
- [20] M. H. Park, T. Schenk, C. M. Fancher, E. D. Grimley, C. Zhou, C. Richter, J. M. LeBeau, J. L. Jones, T. Mikolajick, U. Schroeder, *J. Mater. Chem. C* **2017**, 5, 4677.
- [21] Y. S. Chen, H. Y. Lee, P. S. Chen, P. Y. Gu, C. W. Chen, W. P. Lin, W. H. Liu, Y. Y. Hsu, S. S. Sheu, P. C. Chiang, W. S. Chen, F. T. Chen, C. H. Lien, M.-J. Tsai, in *2009 IEEE International Electron Devices Meeting (IEDM)*, IEEE, Piscataway, NJ **2009**, pp. 1–4.
- [22] E. D. Grimley, T. Schenk, T. Mikolajick, U. Schroeder, J. M. LeBeau, *Adv. Mater. Interfaces* **2018**, 5, 1701258.
- [23] S. Maiti, T. Ohlerth, N. Schmidt, S. Aussen, R. Waser, U. Simon, S. Karthäuser, *J. Phys. Chem. C* **2022**, 126, 18571.
- [24] I. Valov, T. Tsuruoka, *J. Phys. D: Appl. Phys.* **2018**, 51, 413001.
- [25] A. R. Oganov, C. W. Glass, *J. Chem. Phys.* **2006**, 124, 244704.
- [26] A. R. Oganov, A. O. Lyakhov, M. Valle, *Acc. Chem. Res.* **2011**, 44, 227.
- [27] A. O. Lyakhov, A. R. Oganov, H. T. Stokes, Q. Zhu, *Comput. Phys. Commun.* **2013**, 184, 1172.
- [28] X. Sang, E. D. Grimley, T. Schenk, U. Schroeder, J. M. LeBeau, *Appl. Phys. Lett.* **2015**, 106, 162905.
- [29] R. N. Patil, E. C. Subbarao, *J. Appl. Crystallogr.* **1969**, 2, 281.
- [30] K. Z. Rushchanskii, S. Blügel, M. Ležaić, *Phys. Rev. Mater.* **2018**, 2, 115002.
- [31] K. Z. Rushchanskii, S. Blügel, M. Ležaić, *Faraday Discuss.* **2019**, 213, 321.
- [32] K. Z. Rushchanskii, S. Blügel, M. Ležaić, *Phys. Rev. Lett.* **2021**, 127, 087602.
- [33] A. R. Oganov, Y. Ma, A. O. Lyakhov, M. Valle, C. Gatti, *Rev. Mineral. Geochem.* **2010**, 71, 271.
- [34] G. Kresse, J. Hafner, *Phys. Rev. B* **1993**, 47, 558.
- [35] G. Kresse, J. Furthmüller, *Phys. Rev. B* **1996**, 54, 11169.
- [36] G. Kresse, D. Joubert, *Phys. Rev. B* **1999**, 59, 1758.
- [37] J. P. Perdew, K. Burke, M. Ernzerhof, *Phys. Rev. Lett.* **1996**, 77, 3865.
- [38] P. E. Blöchl, *Phys. Rev. B* **1994**, 50, 17953.
- [39] A. V. Krukau, O. A. Vydrov, A. F. Izmaylov, G. E. Scuseria, *J. Chem. Phys.* **2006**, 125, 224106.
- [40] K. Momma, F. Izumi, *J. Appl. Crystallogr.* **2011**, 44, 1272.
- [41] Jülich Supercomputing Centre, *J. Large-Scale Res. Facilities* **2021**, 7, A182.